IV International Conference on Particle-based Methods – Fundamentals and Applications
PARTICLES 2015
E. Oñate, M. Bischoff, D.R.J. Owen, P. Wriggers & T. Zohdi (Eds)

MULTIPHASE ANALYSIS OF STRAIN LOCALIZATION WITH REGULARIZED MODELS

MARIA LAZARI, LORENZO SANAVIA AND BERNHARD A. SCHREFLER

Department of Civil, Architectural and Environmental Engineering (ICEA)
University of Padua (UNIPD)
Via F. Marzolo 9, 35131 Padova, Italy
e-mail: maria.lazari@unipd.it, lorenzo.sanavia@unipd.it, bernhard.schrefler@dicea.unipd.it,
web page: http://www.dicea.unipd.it/

Key words: Viscoplasticity, Non-local approach, Strain localization, Multiphase porous media.

Abstract. In this paper rate-dependent plasticity is employed to regularize, from the scope of mesh independency, the numerical solution in strain localization process of multiphase geomaterials. Towards this goal, an already existing model for multiphase porous media is enhanced with local and non-local elasto-viscoplasticity to obtain mesh insensitive results even in case of weakly rate-sensitive materials where artificial viscosities are needed for the regularization of the numerical solution. The numerical validation and analysis of the regularization properties of both viscoplastic models is illustrated by simulating numerical examples from the geomechanics field like a biaxial strain localization test and a slope stability problem.

1 INTRODUCTION

Computational investigation of natural slopes' stability with a coupled hydro-mechanical approach becomes more and more attractive due to an increasing number of slope movements caused by heavy rainfall events. Basic elements of interest in modelling the initiation of slope failure are the triggering mechanisms and the prediction of the location and the time of occurrence of the failure event. Another element that should be addressed is whether the numerical solution is objective with respect to the spatial discretization of the slope's geometry, especially when applying FEM based on Cauchy continuum to simulate the slope failure with a localized pattern. In such a case a particular care is required, to avoid the dependency of the shear band from the element size upon mesh refinement. It is worth noting that from experimental investigations it has become clear that the width of the shear band is directly connected to a micro-structural length. For instance Roscoe [1], based on direct experimental observations, proposed that the width of shear bands is about 10 times the averaged grain diameter. In addition, as it is addressed by many authors [2,3], strain softening or the use of a non-associated flow rule within the framework of elasto-plasticity theory, cause numerical instabilities and pathological mesh sensitivity.

To overcome these drawbacks, suitable constitutive models containing a characteristic internal length scale related to the observed shear band width can be found in the literature, e.g. rate-dependent constitutive models [4-7] and gradient plasticity models [8]. Alternatively, kinematics has to be enhanced, e.g. by adopting micropolar continuum [9].

The present contribution is dealing with the elimination of mesh sensitivity problems in strain localization simulation of multiphase geomaterials under the scope of realistic modeling of the shear zone thickness in geotechnical applications. Viscoplasticity and non-local theories are employed and implemented in an existing finite element code for multiphase porous media [10-13]. The non-local model is of integral-type and is used in conjunction with viscosity as an extension of an already available viscoplastic Drucker-Prager model with non-associated flow rule [14,27]. This coupling allows for eliminating mesh dependency in strain localization even in case of weakly rate-sensitive materials (i.e. dense sand) for which viscoplasticity is not sufficient to suit numerical requirement of mesh independency [15].

The present study is structured as follows: Section 2 includes the main assumptions and features of the mathematical model for porous media along with a synopsis of the particular characteristics of viscoplasticity and non-local theories. In Section 3 the numerical results coming out from the simulation of a plane strain compression test using local and non-local viscoplasticity are presented, followed by the numerical simulation of a slope failure in Section 4. The conclusions drawn from these investigations are given in Section 5.

2 MULTIPHASE MODEL – A GENERAL DESCRIPTION

In the present work we make use of a mathematic model for non-isothermal variably saturated porous media developed within the Hybrid Mixture Theory [16,17] following [18-21]. For the sake of brevity only a general description of the model with its basic assumptions will be presented hereafter and more details regarding its numerical implementation, for the interested reader, is refereed to [10,13].

In the framework of realistic description of natural geomaterials it is necessary to proceed from an unsaturated soil based on a multiphase model. Therefore, the variably saturated porous medium is treated as a multiphase system consisting of a solid skeleton with open pores filled with liquid water and gas. The gas phase is modelled as an ideal gas composed of dry air (non-condensable gas) and water vapour (condensable gas), which are considered as two miscible species. Phase changes of water (evaporation and condensation) as well as heat transfer through conduction and convection are considered. Furthermore, the non-polar solid is deformable, resulting in a coupling of the fluid, the solid and the thermal fields. All fluid phases are in contact with the solid phase. In the partially saturated zones the liquid water is separated from its vapour by a concave meniscus (capillary water). Due to the curvature of this meniscus, the sorption equilibrium equation [18] gives the relationship, $p^c=p^g-p^w$ between the capillary pressure p^c, gas pressure p^g and liquid water pressure p^w.

The mathematical model consists of four kind of balance equations (mass of dry air, mass of water species, enthalpy of the whole medium and equilibrium equation of the multiphase medium), as well as appropriate constitutive equations for the fluids and solid phase. The balance equations were developed in the geometrically linear framework considering quasi-static loading conditions. The chosen macroscopic primary variables are: gas pressure, capillary pressure, temperature and displacements [13], corresponding to real measurable quantities directly linked to laboratory practice. This is an important aspect when selecting the appropriate constitutive equations.

The governing equations are discretized in space by means of the standard finite element method (Bubnov-Galerkin method) and in time by a fully implicit finite difference scheme

(backward difference) and are solved by means of Newton-Raphson type procedure. Further particulars and general references on the numerical treatment can be found in [10,13].

In the following, direct notation will be adopted. Boldface letters will denote vector or tensors and lightface italic letters will be used for scalar quantities.

2.1 Equilibrium equation

The equilibrium equation of the mixture in terms of generalized effective Cauchy's stress tensor $\boldsymbol{\sigma}'(\boldsymbol{x}, t)$ assumes the form:

$$\operatorname{div}\left(\boldsymbol{\sigma}' - \left[p^g - S_w p^c\right]\mathbf{1}\right) + \rho\mathbf{g} = 0 \tag{1}$$

where $\rho = [1\text{-}n]\rho^s + nS_w\rho^w + nS_g\rho^g$ is the mass density of the overall medium, $n(\boldsymbol{x}, t)$ is the porosity, $S_w(\boldsymbol{x}, t)$ and $S_g(\boldsymbol{x}, t)$ are respectively the water and gas degree of saturation, $\mathbf{g}$ is the gravity acceleration vector and $\mathbf{1}$ is the second order identity tensor.

2.2 Mass balance equations

The mass conservation equation for the mixture of solid skeleton, liquid water and its vapour is:

$$\begin{aligned} & n\left[\rho^w - \rho^{gw}\right]\left[\frac{\partial S_w}{\partial t}\right] + \left[\rho^w S_w + \rho^{gw}\left[1 - S_w\right]\right]\operatorname{div}\left(\frac{\partial \mathbf{u}}{\partial t}\right) \\ & + \left[1 - S_w\right] n \frac{\partial \rho^{gw}}{\partial t} - \operatorname{div}\left(\rho^g \frac{M_\alpha M_w}{M_g^2} \boldsymbol{D}_{\mathrm{g}}^{\mathrm{gw}} \operatorname{grad}\left(\frac{p^{gw}}{p^g}\right)\right) \\ & + \operatorname{div}\left(\rho^w \frac{\mathbf{k}^{\mathrm{w}} k^{rw}}{\mu^w}\left[-\operatorname{grad}(p^g) + \operatorname{grad}(p^c) + \rho^w \mathbf{g}\right]\right) \\ & + \operatorname{div}\left(\rho^{gw} \frac{\mathbf{k}^{\mathrm{g}} k^{rg}}{\mu^g}\left[-\operatorname{grad}(p^g) + \rho^g \mathbf{g}\right]\right) - \beta_{swg} \frac{\partial T}{\partial t} = 0 \end{aligned} \tag{2}$$

where $\mathbf{k}^\pi(\boldsymbol{x}, t) = k^\pi(\boldsymbol{x}, t)\mathbf{1}$ is the intrinsic permeability tensor of the porous matrix in π-fluid saturated condition [m^2], which is assumed to be isotropic, $k^{r\pi}(\boldsymbol{x},t)$ is the fluid relative permeability parameter and $\mu^\pi(\boldsymbol{x}, t)$ is the dynamic viscosity of the fluid [Pa·s], with $\pi = w, g$. $\boldsymbol{D}_{\mathrm{g}}^{\mathrm{gw}}$ is the effective diffusivity tensor of water vapour in the gas phase contained within the pore space, $\beta_{swg} = \beta_s(1\text{-}n)\cdot(S_g\,\rho^{gw} + \rho^w S_w)$ and M_α, M_w and $M_g(\boldsymbol{x},t)$ are the molar mass of dry air, liquid water and gas mixture, respectively. Similarly, the mass balance equation for the dry air is:

$$-n\rho^{g\alpha}\left[\frac{\partial S_w}{\partial t}\right]+\rho^{g\alpha}\left[1-S_w\right]\mathrm{div}\left(\frac{\partial \mathbf{u}}{\partial t}\right)+n\left[1-S_w\right]\frac{\partial \rho^{g\alpha}}{\partial t}-\mathrm{div}\left(\rho^{g}\frac{M_\alpha M_w}{M_g^2}\mathbf{D}_{\mathrm{g}}^{\mathrm{g}\alpha}\mathrm{grad}\left(\frac{p^{g\alpha}}{p^{g}}\right)\right) \tag{3}$$
$$+\mathrm{div}\left(\rho^{g\alpha}\frac{\mathbf{k}^{\mathrm{g}}k^{rg}}{\mu^{g}}\left[-\mathrm{grad}(p^{g})+\rho^{g}\mathbf{g}\right]\right)-\left[1-n\right]\beta_s\rho^{g\alpha}\left[1-S_w\right]\frac{\partial T}{\partial t}=0$$

2.3 Enthalpy balance equation

The enthalpy balance equation of the mixture has the following form:

$$\left(\rho C_p\right)_{eff}\frac{\partial T}{\partial \mathrm{t}}+\rho^{w}C_p^{w}\left[\frac{\mathbf{k}^{\mathrm{w}}k^{rw}}{\mu^{w}}\left[-\mathrm{grad}(p^{g})+\mathrm{grad}(p^{c})+\rho^{w}\mathbf{g}\right]\right]\cdot\mathrm{grad}T \tag{4}$$
$$+\rho^{g}C_p^{g}\left[\frac{\mathbf{k}^{g}k^{rg}}{\mu^{g}}\left[-\mathrm{grad}(p^{g})+\rho^{g}\mathbf{g}\right]\right]\cdot\mathrm{grad}T-\mathrm{div}\left(\chi_{eff}\mathrm{grad}T\right)=-\dot{\mathrm{m}}_{\mathrm{vap}}\Delta\mathrm{H}_{\mathrm{vap}}$$

where, $\rho(C_p)_{eff}$ is the effective thermal capacity of the porous medium, $C_p^w(\boldsymbol{x},t)$ and $C_p^g(\boldsymbol{x},t)$ are the specific heat of the water and gas mixture respectively, and $\chi_{eff}(\boldsymbol{x}, t)$ is the effective thermal conductivity of the porous medium. The right hand side term of Eq. (4) considers the contribution of the evaporation and condensation.

2.4 Constitutive equations

For the gas phase which is assumed to be a perfect mixture of two ideal gases, the state equation of a perfect gas (Clapeyron's equation) and Dalton's law are applied to dry air ($g\alpha$), water vapour (gw) and moist air (g). In the partially saturated zones, the water vapour pressure $p^{gw}(\boldsymbol{x}, t)$ is obtained from the Kelvin-Laplace equation. The saturation $S_\pi(\boldsymbol{x}, t)$ and the relative permeability $k^{r\pi}(\boldsymbol{x},t)$ are experimentally determined functions of the capillary pressure p^c and the temperature T.

The behaviour of the soil skeleton is described within the framework of elasto-viscoplasticity theory for geometrically linear problems. The generalized effective stress state is limited by the Drucker-Prager yield surface with isotropic linear hardening and non-associated plastic flow:

$$f\left(p',\mathbf{s}',\mathrm{q}\right)=3\alpha_f p'+\left\|\mathbf{s}\right\|-\beta_f\sqrt{\frac{2}{3}}\left[\mathrm{c}_0+\mathrm{H}\xi^{\mathrm{vp}}\right] \tag{5}$$

In Eq. (5) p' = (1/3)tr$\boldsymbol{\sigma}$' is the mean effective Cauchy pressure, ||**s**|| is the norm of the deviator effective Cauchy stress tensor $\boldsymbol{\sigma}$', c_0 is the apparent cohesion, α_f and β_f are two material parameters related to the friction angle φ of the soil defined by Eq. (6), H is the hardening/softening modulus and ξ^{vp} is the equivalent viscoplastic strain. The flow rule is of non-associated type, with the plastic potential function given by Eq. (5) but with the dilatancy angle ψ substituting the friction angle in Eq. (6).

$$\alpha_f = 2\frac{\sqrt{2/3}\sin\varphi}{3-\sin\varphi} \quad , \quad \beta_f = 2\frac{6\cos\varphi}{3-\sin\varphi} \tag{6}$$

The total strain rate in an elasto-viscoplastic material is additively decomposed into an elastic and a viscoplastic strain rate:

$$\dot{\boldsymbol{\varepsilon}} = \dot{\boldsymbol{\varepsilon}}^{\mathrm{e}} + \dot{\boldsymbol{\varepsilon}}^{\mathrm{vp}} \tag{7}$$

where the superimposed dot denotes time derivative. Considering linear elasticity, the stress rate is related to the strain rate via the following constitutive relation:

$$\dot{\boldsymbol{\sigma}} = \mathbf{D}^{\mathrm{e}} : \left(\dot{\boldsymbol{\varepsilon}} - \dot{\boldsymbol{\varepsilon}}^{\mathrm{vp}}\right) \tag{8}$$

where $\mathbf{D}^{\mathrm{e}}$ is the fourth-order elastic tensor and double dots ":" denote the doubly contracted tensor product.

In the viscoplastic model proposed by Perzyna [22] (which from this point on will be referred as local to distinguish from non-local), the viscoplastic strain rate is directly linked to the yield function through the viscous nucleus:

$$\dot{\boldsymbol{\varepsilon}}^{\mathrm{vp}} = \gamma \left\langle \Phi\left(\frac{f}{f_0}\right)^{\mathrm{N}} \right\rangle \frac{\partial \mathrm{g}}{\partial \boldsymbol{\sigma}'} \tag{9}$$

with f being the yield function, f_0 introduced as a reference fixed value making the viscous nucleous dimensionless, γ is a fluidity parameter which depends on the viscosity η of the material ($\gamma=1/\eta$), N is a calibration parameter ($N \geq 1$) and g is the viscoplastic potential function. Associative flow is invoked by $g=f$.

In Eq. (9), "$\langle\cdot\rangle$" are the McCauley brackets, such that:

$$\left\langle \Phi(\mathrm{x}) \right\rangle = \begin{cases} \Phi(\mathrm{x}) & \text{if } \Phi(\mathrm{x}) \geq 0 \\ 0 & \text{if } \Phi(\mathrm{x}) < 0 \end{cases} \tag{10}$$

Non-local approach is introduced next because in case of weakly rate-sensitive materials (such as dense sand) artificial viscosities have to be chosen to obtain objective finite element results. To ensure a regularized numerical solution physically based, the local viscoplastic model of Perzyna is expanded with respect to the non-local approach following [25].

According to Jirásek [23] in non-local approach a certain variable, f, is substituted with its non-local counterpart, $\hat{f}$, obtained by weighted averaging over a spatial neighbourhood (distributing points located at ξ) of each point under consideration (located at x):

$$\hat{f}(\mathrm{x}) = \int_{\mathrm{v}} \alpha(\mathrm{x},\xi)\, f(\xi)\mathrm{d}\xi \tag{11}$$

Key points for the formulation and implementation of a non-local approach are the chosen weighting function for the averaging and as non-locality is introduced into the constitutive equations. The weighting function contains at least one parameter with the dimension of length, which incorporates information about the microstructure and controls the size of the localized plastic zone [24]. Herein, inspired by [25], the yield function is chosen to be the

non-local variable and a Gaussian weighting function with a bounded support is selected (Eq.12).

$$\alpha_0(\mathbf{x}-\boldsymbol{\xi}) = \begin{cases} \exp\left(-\dfrac{2\cdot(\mathbf{x}-\boldsymbol{\xi})}{l}\right)^2 & \text{if } \|\mathbf{x}-\boldsymbol{\xi}\| \le R \\ 0 & \text{if } \|\mathbf{x}-\boldsymbol{\xi}\| > R \end{cases} \tag{12}$$

Choosing yield function as the non-local variable, the viscous nucleus and consequently the viscoplastic flow rule are modified:

$$\dot{\boldsymbol{\varepsilon}}^{vp} = \gamma\Phi\left(\hat{f}\right)\frac{\partial g}{\partial \boldsymbol{\sigma}'} \tag{13}$$

3 PLANE STRAIN COMPRESSION TEST

In this section, local and non-local viscoplasticity is applied to a biaxial strain compression test of an initially water saturated, globally undrained dense Hostun RF sand, where strain localization and cavitation (phase change of the liquid water to vapour) were experimentally observed. This numerical example was previously studied by Sanavia et al. [13], inspired by the experimental work of [26], assuming a rate-independent behaviour for the description of the mechanical behaviour of sand.

Herein, mesh sensitivity of the numerical results is examined by using two different finite element discretizations. The adopted meshes consist of 340 (10x34) and 1360 (20x68) elements respectively, for a rectangular sample of homogeneous soil of 34 cm height and 10 cm width. The finite element mesh consists of eight node quadrilateral isoparametric elements with reduced Gaussian (2x2) integration scheme. The bottom of the sample was assumed to be fixed and rough, whereas the boundaries are impervious and adiabatic. Quasi-static loading conditions are assumed and gravity acceleration is taken into account. Axial compression is applied to the specimen by imposing vertical velocity (v=1.2 mm/s) on the top. No weak elements are specified since the boundary value problem inherently generates a non-uniform stress field. The material parameters used in the computation are as in [13].

For brevity, indicative results are presented for the sake of comparison of the proposed methods. A more detailed presentation and analysis of the influencial parameters of the problem, such the loading velocity, the value of permeability and the interaction of the internal lengths (introduced by viscosity and non-locality) can be found in [27].

The numerical validation of both models in the Comes-geo [10,13] code is first presented. In Figure 1a are plotted the equivalent inelastic strains in the vertical section at the centre of the sample for both elastoplastic (solid line) and elasto-viscoplastic (square markers) constitutive models to verify that for rather small values of viscosity elastoplastic limit is approached [28]. The comparison of the results shows the coincedence between the elastoplastic and the considered viscoplastic solution for nil viscosity value. In addition, in Fig. 1b it is observed that for small values of the internal length l, the non-local solution approaches the local one. The difference between the non-local and the local elasto-viscoplastic solution tends to disappear for very small values of l, owing to the fact that in such a case only one integration point may be inside the interaction radius where the non-local

averaging is performed.

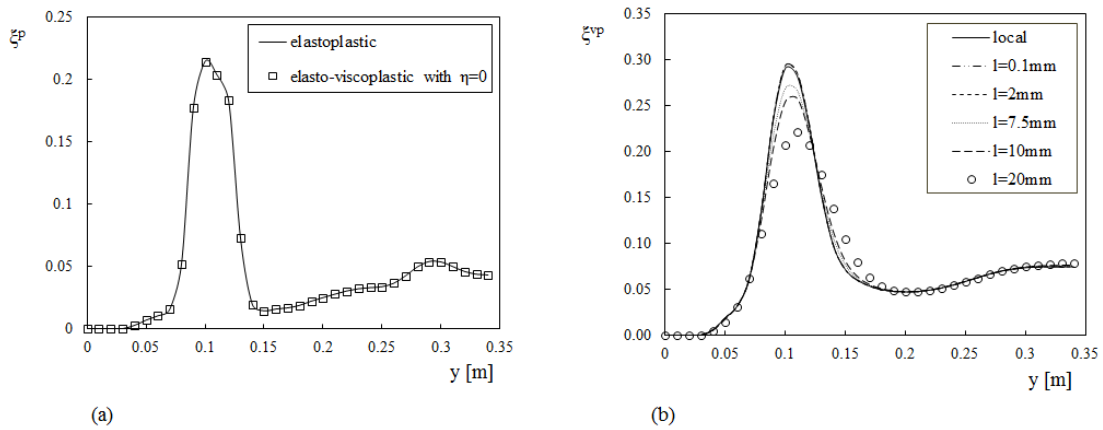

Figure 1: Numerical validation of (a) local and (b) non-local elasto-viscoplastic Perzyna model in Comes-geo code (10x34 mesh).

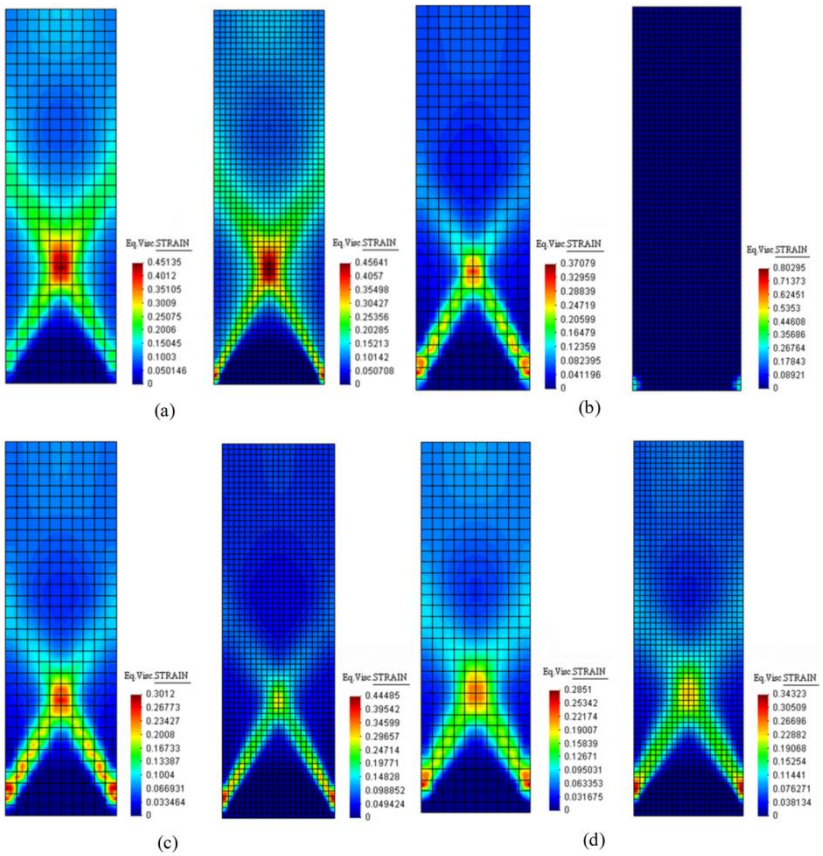

Figure 2: Numerical results for (a) local viscoplasticity with η=30s, (b) local viscoplasticity with η=10s, (c) non-local viscoplasticity with η=10s, l=0.01m and (d) non-local viscoplasticity with η=10s, l=0.02m, for two meshes (10x34 and 20x68 respectively).

The effect of the local and non-local elasto-viscoplastic model of Perzyna in the regularization of the mesh dependency problem is illustrated in Fig. 2. The influence of the viscosity parameter, η, is clearly depicted for the local elasto-viscoplastic model. In the case of η=30s, a regularized solution is obtained for both meshes: the shear band width remains unaltered upon mesh refinement and the peak value of equivalent viscoplastic strain coincides for the two meshes. However, considering a less rate-sensitive material with η=10s (and as approaching the elastoplastic limit), the regularizing effect of the local elasto-viscoplastic model is lost and the contour of the more refined mesh reveals strong mesh-sensitivity (Fig. 2b). In this case, the non-local elasto-viscoplastic model proves to be sufficient to regularize the finite element solution for the given material parameters and the shear band propagates for internal length value, l=0.01m (Fig. 2c). Moreover, in the case of internal length value l=0.02m (Fig. 2d), the width of the shear band increases accordingly to the l value for both meshes adopted.

In Fig. 3 the numerical solution for the liquid phase is presented in terms of capillary pressure and water saturation. The results are presented for the case of non-local elasto-viscoplastic plastic model, and mesh independency is apparent also for the fluid part. It is evident that pore water decreases up to the development of capillary pressure, accompanied by desaturation in the strain localization zones. It is noted that at the same time water pressure decreases below the vapour saturation pressure and the phase change of the liquid water to vapour occurs.

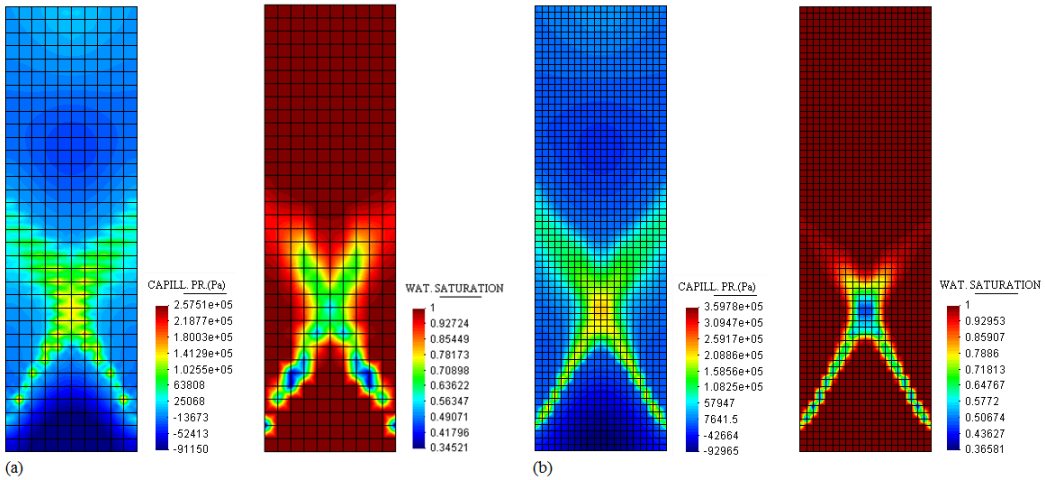

Figure 3: Non-local approach: Capillary pressure and water degree of saturation contours for (a) 10x34 mesh and (b) 20x68 mesh, in case of l=7.5mm and η=10s.

4 SLOPE STABILITY TEST

A slope stability problem, inspired by Regueiro and Borja [29], is now presented to demonstrate the effectiveness of adopting the regularization techniques developed in this work. The dimensions and boundary conditions of the problem are shown in Fig. 4 whereas the soil parameters considered in the analysis are indicated in Table 1. The initial stress field is given by geostatic stress state; drained conditions are imposed. Next, a downward displacement with a constant rate of 10^{-3} m/s is applied on a portion of 4m on the top slope

surface (Fig. 4). Two meshes with 400 and 1600 eight node quadrilateral isoparametric elements are used to analyze the problem. The analyses are performed using: the elastoplastic model, the local elasto-viscoplastic model of Perzyna with viscosity η=100s and the non-local elasto-viscoplastic model with an internal length of l=0.8 m. The results from these models are compared in Fig. 5 in terms of equivalent (visco)plastic strain and in Fig. 6 with the force-displacement plots.

Table 1: List of soil parameters for the slope stability problem.

E [MPa]	ν	γ [kN/m^3]	c_0 [kPa]	φ [°]	ψ [°]	h [kPa]	n	k [m^2]
10	0.4	20	40	10	3	-10	0.3	1E-10

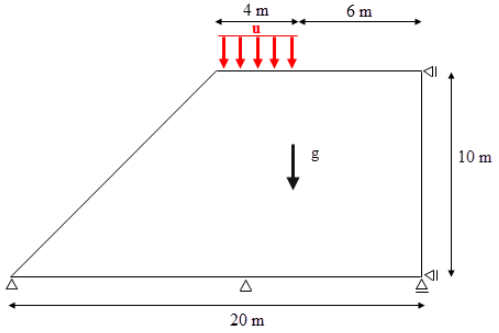

Figure 4: Slope stability problem. Geometry and boundary conditions.

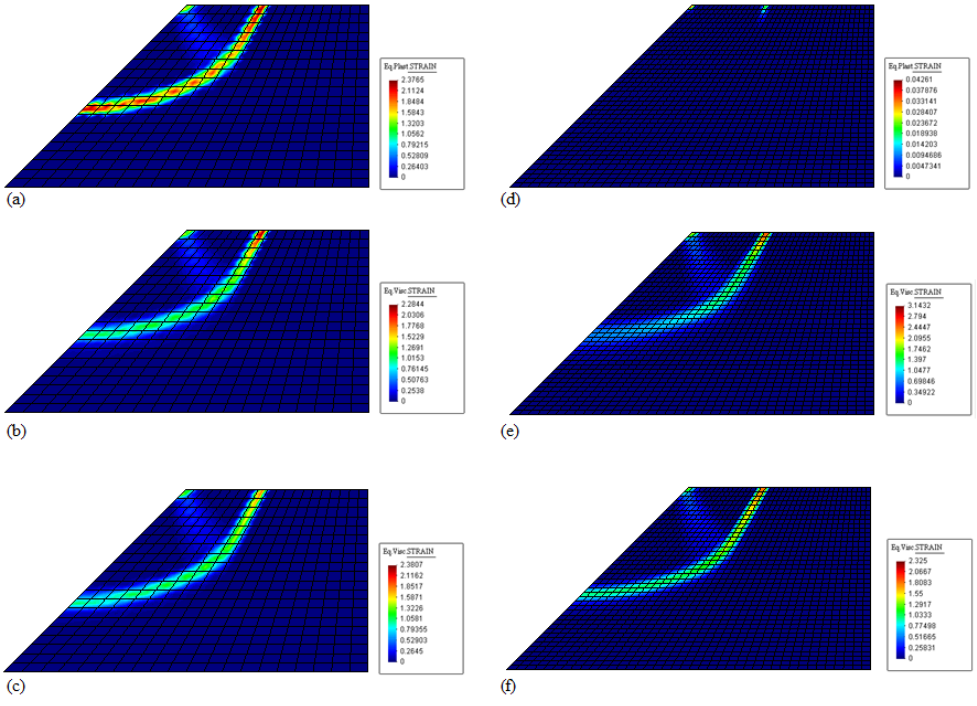

Figure 5: Equivalent (visco)plastic strain contours as calculated using the elastoplastic model (a,d), the local elasto-viscoplastic model (b,e) and the non-local elasto-viscoplastic model (c,f) for a mesh of 400 elements (a), (b) and (c) and for a mesh of 1600 elements (d), (e) and (f), respectively.

The failure initiates in the element just to the right of the applied force and propagates in a manner depended on the angle of friction. When the elastoplastic constitutive model is used to solve this initial boundary value problem, a classical mesh dependent numerical solution is observed with the model being unable to simulate the failure process of the slope when the mesh is refined (Fig. 5d). As is shown in Fig. 6b when the elasto-viscoplastic formulation of Perzyna is adopted, even if the number of elements is increased, the shear band formation and the force-displacement relationship are not affected by the element size. However, the peak value of the viscoplastic strain field depends on the element size of the mesh (Fig. 5e). Finally, the non-local elasto-viscoplastic model is able to predict a clearly defined shear band and the slope's strain-softening response (Fig. 6c) independently of the mesh adopted (Fig. 5f).

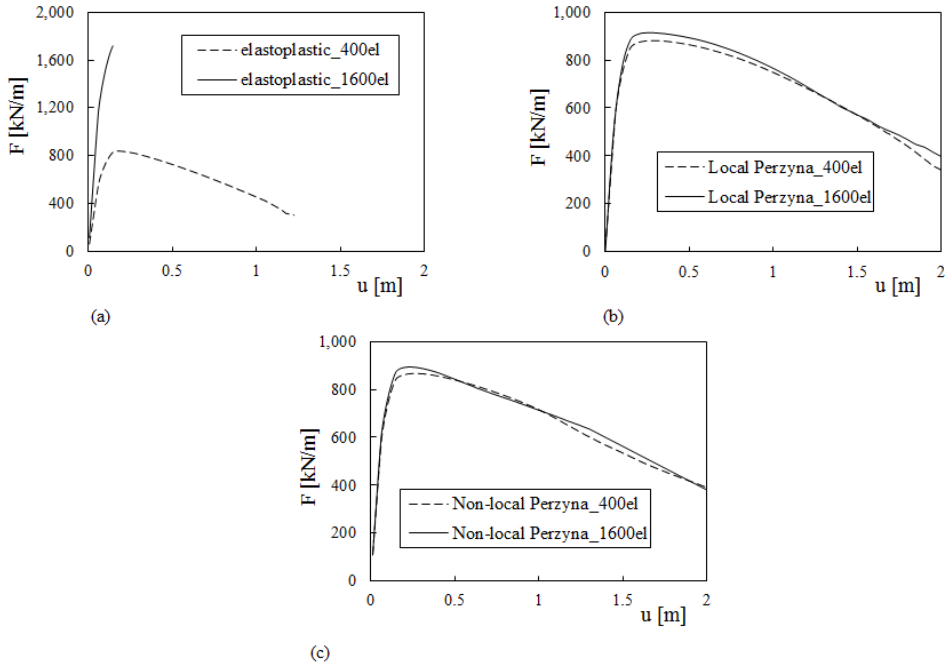

Figure 6: Force-displacement plots for (a) the elastoplastic model, (b) the local elasto-viscoplastic model and (c) the non-local elasto-viscoplastic model, for the two meshes.

5 CONCLUSIONS

In this work the mesh sensitivity problem in strain localization simulation of multiphase geomaterials is overcomed by means of viscoplasticity and nonlocal theory. These formulations are implemented in an existing finite element code for multiphase porous media. Both methods introduce a characteristic length scale (implicitly and explicitly) which prevents strains from localizing into infinitely narrow bands when the mesh is refined.

The validation of the implementation of the methods is presented and the effectiveness of the methods is studied, within the framework of an undrained biaxial test. The initiation and the propagation of the shear band are effectively described by means of FEM analysis, regardless of the mesh size adopted. The strain localization process realistically occurs within the shear band failure mode and its size is governed by the viscosity parameter and the

internal length variable, which can be directly estimated by experimental tests. The rate sensitivity of the material is investigated showing the holistic confrontation of the strain localization phenomenon by the combination of the two methods.

The efficiency of the models in terms of regularized performance is also illustrated using a numerical example of a slope failure problem. The numerical results indicate that only by using the applied regularization techniques the location and the propagation of the shear zone is reliably simulated in a mesh independent manner.

ACKNOWLEDGMENT

The authors would like to thank the 7th Framework Programme of the European Union (ITN MuMoLaDe project 289911) for the financial support of this work.

REFERENCES

[1] Roscoe, K.H. The influence of strains in Soil Mechanics. *Géotechnique* (1970) **20**:129-170.

[2] Nova, R. The role of non-normality in soil mechanics and some of its mathematical consequences. *Computers and Geotechnics* (2004) **31**:185–191.

[3] Rudnicki, J.W and Rice, J.R. Conditions for the localization of deformation in pressure-sensitive dilatant materials. *Journal of the Mechanics and Physics of Solids* (1975) **23**:371-394.

[4] Ehlers, W., Graf, T. and Ammann, M. Deformation and localization analysis of partially saturated soil. *Computer Methods in Applied Mechanics and Engineering* (2004) **193**:2885–2910.

[5] Loret, B. and Prevost, J.H. Dynamic strain localization in fluid-saturated porous media. *Journal of Engineering Mechanics* (1991) **117**(4):907-922.

[6] Schrefler, B.A., Zhang, H.W. and Sanavia, L. Fluid-structure interaction in the localization of saturated porous media. ZAMM Zeitschrift für Angewandte Mathematik und Mechanik, *Journal of Applied Mathematics and Mechanics. Z. Angew. Math. Mech.* (1999) **79**:481-484.

[7] Schrefler, B.A, Zhang, H.W and Sanavia, L. Interaction between different internal length scales in fully and partially saturated porous media – The 1-D case, *International Journal for Numerical and Analytical Methods in Geomechanics* (2006) **30**:45-70.

[8] Zhang, H.W and Schrefler, B.A. Gradient-dependent plasticity model and dynamic strain localization analysis of saturated and partially saturated porous media: one dimensional model. *European Journal of Mechanics A/Solids* (2000) **19**(3):503–524.

[9] Ehlers, W. and Volk, W. On theoretical and numerical methods in the theory of porous media based on polar and non-polar elasto-plastic solid materials. *International Journal of Solids and Structures* (1998) **35**:4597-4617.

[10] Gawin, D. and Schrefler, B.A. Thermo-hydro-mechanical analysis of partially saturated porous materials. *Engineering Computations* (1996) **13**(7):113-143.

[11] Gawin, D. and Sanavia, L. A unified approach to numerical modelling of fully and partially saturated porous materials by considering air dissolved in water. *CMES-Comp. Model. Eng. Sci.* (2009) **53**:255-302.

[12] Gawin, D. and Sanavia, L. Simulation of cavitation in water saturated porous media

considering effects of dissolved air. *Transport Porous Media* (2010) **81**:141-160.
[13] Sanavia, L., Pesavento, F. and Schrefler, B.A. Finite element analysis of non-isothermal multiphase geomaterials with application to strain localization simulation. *Computational Mechanics* (2006) **37**:331-348.
[14] Lazari, M., Sanavia, L. and Schrefler, B.A. Viscoplastic regularization of strain localization in fluid-saturated porous media. *Proceedings of WCCM XI-ECCM V*, Tomo IV: 3495-3503, Barcelona, (2014). ISBN: 978-84-942844-7-2
[15] di Prisco, C., Imposimato, S. and Aifantis, E.C. A visco-plastic constitutive model for granular soils modified according to non-local and gradient approaches. *International Journal for Numerical and Analytical Methods in Geomechanics* (2002), **26**:121-138.
[16] Lewis, R.W. and Schrefler, B.A. *The Finite Element Method in the Static and Dynamic Deformation and Consolidation of Porous Media*, Wiley and Sons: Chichester, (1998).
[17] Schrefler, B.A. Mechanics and thermodynamics of saturated/unsaturated porous materials and quantitative solutions. *Applied Mechanics Reviews* (2002) **55**(4):351-388.
[18] Gray, W.G. and Hassanizadeh, M. Unsaturated flow theory including interfacial phenomena. *Water Resources Research* (1991) **27**:1855-1863.
[19] Hassanizadeh, M and Gray, W.G. General conservation equations for multi-phase system: 1. Averaging technique. *Advances in Water Resources* (1979a) **2**:131-144.
[20] Hassanizadeh, M and Gray, W.G. General conservation Equations for multi-phase system: 2. Mass, momenta, energy and entropy equations. *Advances in Water Resources* (1979b) **2**:191-201.
[21] Hassanizadeh, M. and Gray, W.G. General conservation equations for multi-phase systems: 3. Constitutive theory for porous media flow. Advances in Water Resources (1980) **3**(1):25-40.
[22] Perzyna, P. Fundamental problems in viscoplasticity. *Advances in Applied Mechanics* (1966) **9**:243-377.
[23] Jirásek, M. Objective modeling of strain localization. *Revue Française de Genie Civil* (2002) **6**:1119-1132.
[24] Jirásek, M. and Rolshoven, S. Comparison of integral-type nonlocal plasticity models for strain-softening materials. *International Journal of Engineering Science* (2003) **41**:1553-1602.
[25] di Prisco, C. and Imposimato, S. Nonlocal numerical analyses of strain localization in dense sand. *Mathematical and Computer Modelling* (2003) **37**:497-506.
[26] Mokni, M. and Desrues, J. Strain localisation measurements in undrained plane-strain biaxial tests on hostun RF sand. *Mechanics of Cohesive-Frictional Materials* (1998) **4**:419–441.
[27] Lazari, M., Sanavia, L. and Schrefler, B.A. Local and non-local elasto-viscoplasticity in strain localization analysis of multiphase geomaterials. *International Journal for Numerical and Analytical Methods in Geomechanics* (2015), in print.
[28] Needleman, A. Material rate dependence and mesh sensitivity on localization problems. *Computer Methods in Applied Mechanics and Engineering* (1988) **67**:69-86.
[29] Regueiro, R.A. and Borja, R.I. Plane strain finite element analysis of pressure sensitive plasticity with strong discontinuity. *International Journal of Solids and Structures* (2001) **38**:3647-3672.